THE JOURNAL OF PHYSICAL CHEMISTRY B

Article

pubs.acs.org/JPCB

Effect of Temperature and Cationic Chain Length on the Physical Properties of Ammonium Nitrate-Based Protic Ionic Liquids

S. Bouzón Capelo,[†] T. Méndez-Morales,[†] J. Carrete,[†] E. López Lago,[‡] J. Vila,[§] O. Cabeza,[§] J. R. Rodríguez,[†] M. Turmine,[∥] and L. M. Varela*[,†]

[†]Grupo de Nanomateriales y Materia Blanda, Departamento de Física de la Materia Condensada, Universidade de Santiago de Compostela, Campus Vida s/n E-15782, Santiago de Compostela, Spain

[‡]Grupo de Microóptica y Sensores de Frente de Onda, Departamento de Física Aplicada, Universidade de Santiago de Compostela, Campus Vida s/n E-15782, Santiago de Compostela, Spain

[§]Facultad de Ciencias, Universidade de A Coruña, Campus A Zapateira s/n. E-15008, A Coruña, Spain

[∥]Université Pierre et Marie Curie-PARIS6, Laboratoire Interfaces et Systèmes Electrochimiques, CNRS, UPR15-LISE, Paris, F-75005 France

ABSTRACT: We report a systematic study of the effect of the cationic chain length and degree of hydrogen bonding on several equilibrium and transport properties of the first members of the alkylammonium nitrate protic ionic liquids (PILs) family (ethylammonium, propylammonium, and butylammonium nitrate) in the temperature range between 10 and 40 °C. These properties were observed by means of several experimental techniques, including density, surface tension, refractometry, viscosimetry, and conductimetry. The dilatation coefficients and compressibilities, as well as the Rao coefficients, were calculated, and an increase of these magnitudes with alkyl chain length was detected. Moreover, the surface entropies and enthalpies of the studied PILs were analyzed, and the temperature dependence of the surface tension was observed to be describable by means of a harmonic oscillator model with surface energies and critical temperatures that are increasing functions of the cationic chain length. Moreover, the refractive indexes were measured and the thermo-optic coefficient and Abbe numbers were calculated, and the contribution of the electrostrictive part seemed to dominate the temperature dependence of the electric polarization. The electric conductivity and the viscosity were measured and the influence of the degree of hydrogen bonding in the supercooled liquid region analyzed. Hysteresis loops were detected in freezing−melting cycles and the effect of the length of the alkyl chain of the cation on the size of the loop analyzed, showing that longer chains lead to a narrowing of the supercooled region. The temperature dependence of the conductivity was studied in the Vogel−Fulcher−Tamman (VFT) framework and the fragility indices, the effective activation energies, and the Vogel temperatures obtained. A high-temperature Arrhenius analysis was also performed, and the activation energies of conductivity and viscosity were calculated, showing that these transport processes are governed by two distinct mechanisms. The exponents of the fractional Walden rule for the different compounds were obtained. Finally, the ionicities and fragilities of the studied PILs were analyzed, proving that all the studied PILs are subionic and fragile liquids, with propylammonium nitrate showing the lowest fragility and the greater ionicity of all the studied compounds.

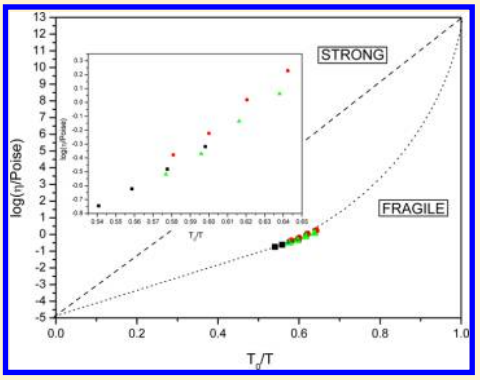

INTRODUCTION

Ionic liquids (ILs) are chemical compounds formed solely by ions and having melting points below 100 °C, but most usually around or below room temperature, which are known to exhibit tunable properties that confer them a central role as "designer solvents", ranging from negligible vapor pressure or the ability to dissolve many inorganic, organic, and polymeric materials at very high concentrations to non-corrosiveness or low flammability. Although it was as early as 1914 that Walden described the synthesis of ethylammonium nitrate, believed to be the first example of a room temperature molten salt, it was not until the early 1990s that Wilkes et al.[1] synthesized air- and water-stable ionic liquid (IL) $[C_2MIM][BF_4]$ (1-ethyl-3-methylimidazolium tetrafluoroborate), opening the gate to a new era in solvents and in the so-called "green" branch of contemporary chemistry. Since then, ILs or room-temperature molten salts have come to be considered novel materials of extreme importance for both academic and industrial purposes.

Protic ILs (PILs) are a subset of ILs characterized by the transfer of a proton from the acid to the base that gives rise to the presence of proton-donor and proton-acceptor sites. Therefore, hydrogen-bond networks are formed in bulk PILs, which confers the whole category a unique set of properties. Together with other interesting features, PILs exhibit the

Received: July 5, 2012
Revised: August 4, 2012
Published: September 5, 2012

   dx.doi.org/10.1021/jp3066822 | J. Phys. Chem. B 2012, 116, 11302−11312

capability of supporting amphiphilic self-assembly,[2−4] although aprotic ILs (AILs) are also known to be able to support the formation of self-assembly mesomorphic aggregates.[5] Alkylammonium nitrates are among the most frequently used PILs. An accurate knowledge of the structure and properties of these liquids is essential for the understanding of their properties, particularly their degree of hydrogen bonding and, consequently, their ability to support structural self-assembly. Specifically, as it is very well-known from studies of aqueous solutions, the formation of aggregates is the result of the balance between energetic (Tanford's opposing forces, hydrophobic attractions of the chains and repulsions of the polar heads), and (mainly) entropic contributions associated with the breakdown of the hydrogen-bonded network of water molecules upon aggregation. Thus, the spontaneity of the hydrophobic effect is highly dependent on temperature, and in fact below a definite temperature known as Krafft's temperature, micellization is no longer possible. Moreover, these liquids are also frequently employed as electrolytes in fuel cells, as solvents for proteins, and in biocatalysis among other uses (see the excellent review of Greaves and Drummond in ref 3 and references therein). Thus, an adequate knowledge of the temperature dependence of the physical properties of these PILs is crucial for their usage in many processes, particularly for electrochemical and self-association purposes.

However, to the best of our knowledge, no systematic study of the temperature dependence of the equilibrium and transport physical properties of the alkylammonium nitrate family at near-ambient temperatures has been reported yet. In this paper, we report experimental measurements of several thermodynamic and transport properties of ethylammonium (EAN), propylammonium (PAN), and butylammonium (BAN) nitrates, the latter a relatively new compound whose synthesis was reported for the first time as far as we know in 2010,[6] and we analyze their dependence on temperature and on the length of the radical chain, emphasizing the role of hydrogen bonding on the experimental observations. Particularly, we report measurements of volumetric properties, surface tension, optical properties, electric conductivities, freezing−melting cycles, and viscosities. Moreover, we analyze the ionicities and fragilities of the studied PILs from the Walden and fragility plots, respectively. To our knowledge, most of them have never been reported for the compound with the longer chain length, BAN.

In the section after this introduction, we describe the main features of the experimental procedures followed for the measurement of the reported experimental data. The following section contains the results and the associated discussion; finally, our main conclusions are summed up.

EXPERIMENTAL SECTION

Chemicals. Ethylammonium nitrate (EAN) and propylammonium nitrate (PAN) (see Scheme 1) were purchased from IOLITEC with purity degrees of >97% and >98%, respectively, and they were used as received. Butylammonium nitrate (BAN) was prepared by adding nitric acid (68.5 wt % in water, VWR, RP) to a cooled solution of butylamine (99%, Aldrich) in water (approximately 75 wt %). The vessel was cooled to −4 °C with a cryothermostat. After reaction, water was removed first with a rotary evaporator and then by freeze-drying.

Density and Ultrasound Velocity Measurements. Density and speed of sound were continuously, simultaneously, and automatically measured at 298.15 K using a DSA 5000

Scheme 1. (a) Ethylammonium Nitrate, (b) Propylammonium Nitrate, and (c) Butylammonium Nitrate

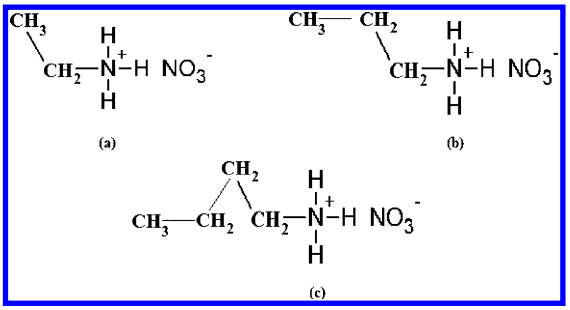

Anton Paar density and sound velocity analyzer. This apparatus is equipped with a latest-generation vibrating tube for density measurements and a stainless-steel cell connected to a sound velocity analyzer with resolutions of $\pm 10^{-6}$ g cm^{-3} and 10^{-2} m s^{-1}, respectively. Both the speed of sound and density are extremely sensitive to temperature, so the latter was controlled to within $\pm 10^{-3}$ K by means of a Peltier module. The reproducibility of density and ultrasound measurements was $\pm 10^{-6}$ g cm^{-3} and 10^{-1} m s^{-1}, respectively. The density meter was calibrated with dry air and distilled water at known pressure and temperature.

Surface Tension Measurements. Both surface tension and refractive index measurements were made in two different laboratories (Santiago de Compostela and A Coruña) to ensure reproducibility. In the laboratory in Santiago, the surface tension of our probe systems was measured by means of a drop volume method using a Lauda TVT2 tensiometer with a 2.5 mL syringe and a capillary tube of inner radius 1.345 mm. The drop volume is measured with an accuracy of ± 0.1 μm. We carried out measurements in a temperature interval from 10 to 40 °C. Temperature was controlled using an external Julabo F10/MH thermostatic bath with a resolution of 0.1 K. In the A Coruña laboratory, surface tension measurements were made by means of a similar drop volume tensiometer, but in that case of model Lauda TVT1, which uses the same syringe and capillary tube dimensions. Temperature was maintained constant with a Haake external bath, providing an accuracy better than 0.1 K. Both apparatuses have a sensitivity of 10^{-5} N·m^{-1}. In addition, any single measurement was performed at least two times to ensure reproducibility, which was better than 5×10^{-5} N·m^{-1}.

Refractive Index Measurements. Refractive indices of the studied compounds for the D line of sodium (λ_D = 589.3 nm) were measured in Santiago using a Zuzi refractometer model 325, with a resolution of 5×10^{-4} for the yellow line of sodium. Temperature control during the refractive index measurements was achieved by means of the Peltier cell of the apparatus with a precision better than 0.1 K at T = 298.15 K. To ensure reproducibility, in A Coruña, refractive indices were measured using an Anton Paar Abbemat WR refractometer, also for the D line of sodium, with a resolution of 10^{-5} and an accuracy of 4×10^{-5}.

Viscosity and Electric Conductivity Measurements. Viscosity measurements were obtained by means of an Anton Paar automatic microviscosimeter, and measurements performed in a temperature interval from 10 to 40 °C, controlled automatically by the equipment. We employed two measuring system sets: the first one equipped with a capillary tube of diameter 1.8 mm and a ball of diameter 1.5 mm was used to

dx.doi.org/10.1021/jp3066822 | J. Phys. Chem. B 2012, 116, 11302−11312

obtain viscosities up to 70 mPa s^{-1}, and the second one, with diameters of 4.0 and 3.0 mm, respectively, for higher viscosities.

Electric conductivity was measured at a constant frequency of 500 Hz using a conductimeter from CRISON, model GLP31. We used two different measuring cells, one with a cell constant $C \approx 1$ cm^{-1} (appropriate for measuring ionic conductivity values from 5×10^{-3} to 200 mS·cm^{-1}) and another one with $C \approx 0.1$ cm^{-1} (to measure values from 2×10^{-6} to 0.5 mS·cm^{-1}). The resolution of the conductimeter with the indicated measuring cells (and within the corresponding range) is better than 1% of the measured value (with a minimum resolution of 2×10^{-6} mS/cm). All data presented here were measured several times in different samples to ensure its reproducibility, which was better than 5% in absolute value. Both measuring cells are formed by two parallel plane plates covered with platinum oxide, and were used to measure conductivities in both phases, liquid and solid. The temperature of the samples was controlled using a Julabo F25 thermostat calibrated with an external sensor Crison T-637, which provided a precision better than 0.1 K in the range of temperature measured. It is important to note that all measurements were done by means of a static isothermal method; thus, the sample was allowed to spend about 15 min at constant temperature before any single measurement was performed, while at the phase transition that period was increased to at least 30 min.

RESULTS AND DISCUSSION

Figure 1a presents the temperature dependence of the density (ρ) of EAN, PAN, and BAN in the temperature range from 10 to 40 °C. A linear dependence on temperature is registered for all the studied PILs. The main effects that we can observe in this representation are as follows: (i) the slope of the density is approximately independent of the cationic chain length in the studied temperature range, and (ii) the density decreases at constant temperature as the alkyl chain length is increased, contrary to the usual trend observed in alkanes. This is consistent with what has been observed previously for other PILs and AILs.[3] This fact is related to the increasing difficulties for packing and hydrogen bonding associated with the size and asymmetry of the ions as the length of the alkyl chain of the cation increases. To understand this behavior, one must recall that each C_nAN (n = 2, 3, 4) can form three $^{+}NH\cdots O^{-}$ hydrogen bonds. However, increasing the alkyl chain length increases the average distance between ions and makes the formation of these hydrogen bonds difficult. The increased repulsions arising from the greater size of the hydrocarbon chains prevents the ions from approaching at distances lower than that of hydrogen bonding, so PILs with shorter alkyl chains are expected to be more hydrogen bonded and, therefore, denser. This fact was also pointed out by Hirao et al.,[7] who stated that decreasing the cation size lowers the glass transition temperature of the ILs through decreasing the packing and cohesive energy of the salts.

From density measurements, the thermal expansion coefficient can be obtained using conventional thermodynamics as

$$\alpha = \frac{1}{V}\left(\frac{\partial V}{\partial T}\right)_P = -\frac{1}{\rho}\left(\frac{\partial \rho}{\partial T}\right)_P \quad (1)$$

which is shown in Figure 1b. As can be seen, as the chain length increases, the thermal expansion coefficient increases, reflecting the lower hydrogen bonding degree of the PILs with the longer

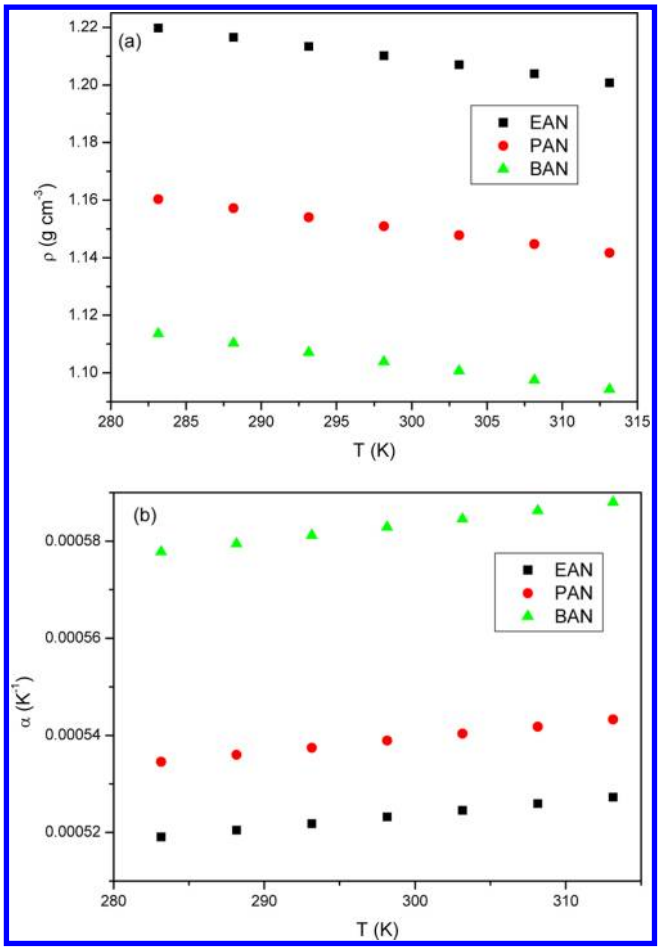

Figure 1. Temperature dependence of the density (a) and thermal expansion coefficient (b) of EAN, PAN, and BAN.

chains. However, the variation of α with the cationic chain length is not linear, since the change in its magnitude from EAN to PAN is approximately 3%, but there is almost an 8% variation registered between PAN and BAN.

Figure 2 shows the thermal behavior of the speed of sound (v) in the hereby reported ILs, Figure 2a, together with the adiabatic compressibility of these systems in Figure 2b calculated by means of the well-known Laplace equation

$$K_s = \frac{1}{\rho v^2} \quad (2)$$

This magnitude increases with temperature in all the studied cases, as expected, given the inverse relation of K_s with structural order. Moreover, it can be observed in Figure 2b that the isentropic compressibility increases with the alkyl chain length in an almost constant fashion, reflecting once more the fact that more asymmetric ILs are less densely packed and thus have looser structures due to a reduction in the degree of hydrogen bonding. Combining these results with the density measurements above, we can also obtain the so-called Rao coefficient[8]

$$K = \frac{\frac{1}{v}\left(\frac{\partial v}{\partial T}\right)_P}{\frac{1}{\rho}\left(\frac{\partial \rho}{\partial T}\right)_P} \quad (3)$$

dx.doi.org/10.1021/jp3066822 | J. Phys. Chem. B 2012, 116, 11302−11312

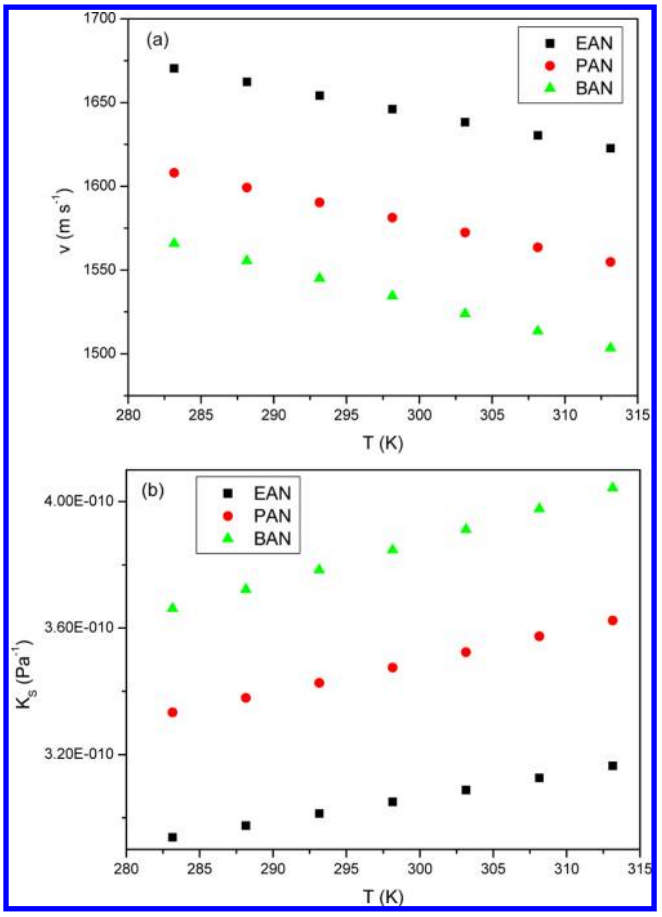

Figure 2. Temperature dependence of the speed of sound (a) and the adiabatic compressibility (b) of EAN, PAN, and BAN.

which is expected to be constant and equal to 3. Despite the fact that this equality does not exactly hold in most liquids, this coefficient is interesting, since it can be approximately related to the exponent of the repulsive part of the interparticle Mie potential $V(r) = ar^{-n} + br^{-m}$, since Nozdrev[9] proved that $n = 2K$, under the assumption of a constant ratio of specific heats and an equation of state

$$PV = k_B T - V\left(\frac{\partial v}{\partial V}\right) \tag{4}$$

Moreover, Rao's coefficient was related by Hartmann[10] to the parameter of nonlinearity of the liquid as $B/A = 2K$, where A and B are the first coefficients of the isentropic equation of state[10]

$$P - P_0 = A\frac{\rho - \rho_0}{\rho_0} + \frac{B}{2}\left[\frac{\rho - \rho_0}{\rho_0}\right]^2 + \ldots \tag{5}$$

Table 1 shows the values of Rao's constant in the studied temperature range. As one can see, this coefficient is remarkably constant with temperature—in contrast to previously reported results for other liquids—but also notably lower than its theoretical value of 3, as has also been reported for molecular liquids such as Freon 114B-2 or Fluorolube at 0 °C.[11] Moreover, Rao's constant increases with the cation alkyl chain length and also slightly with temperature for each compound—this increase being larger the larger the cationic chain length is—reflecting, according to Nozdrev's predictions, shorter

Table 1. Temperature Dependence of the Rao Coefficients in eq 3 for the Compounds Studied in the Paper

T (K)	EAN	PAN	BAN
283.15	1.84	2.07	2.30
288.15	1.85	2.08	2.30
293.15	1.85	2.08	2.32
298.15	1.86	2.09	2.33
303.15	1.86	2.09	2.34
308.15	1.86	2.10	2.34
313.15	1.87	2.11	2.35

range repulsive potentials in ILs with longer cationic side chains.

In regard to Figure 3a, it shows the temperature dependence of the surface tension of the three ILs considered in this paper.

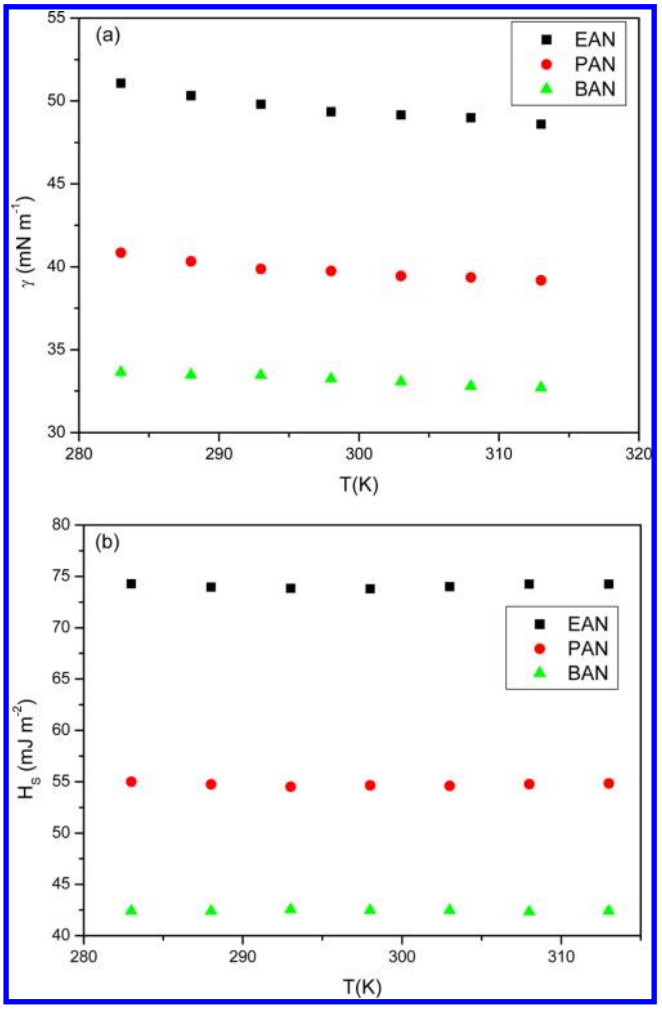

Figure 3. Temperature dependence of the (a) surface tension and (b) surface enthalpy of EAN, PAN, and BAN.

As we can see, this magnitude exhibits an almost linear dependence with temperature, and decreases with the chain length of the cation. Once more, this is in agreement with a decrease in hydrogen bonding associated with an increase of the length of the cationic chain length, which reduces the energetic requirements for the deformation of the IL−air surface. As it is well-known from thermodynamics, surface tension at constant temperature and pressure equals the specific Gibbs free energy per surface area

dx.doi.org/10.1021/jp3066822 | J. Phys. Chem. B 2012, 116, 11302−11312

$$\gamma = \left(\frac{\partial G}{\partial A}\right)_{T,P,n} \quad (6)$$

so the surface tension curve is related to the entropy and enthalpy per unit area by the relations

$$-S^A = \left(\frac{\partial \gamma}{\partial T}\right)_{P,A}$$

$$H^A = \gamma - T\left(\frac{\partial \gamma}{\partial T}\right)_{P,A} \quad (7)$$

The entropies per unit area and temperature calculated from the measured data are approximately temperature-independent throughout the studied temperature range, and their calculated values were 0.082, 0.052, and 0.031 mN m^{-1} K^{-1}, respectively, for EAN, PAN, and BAN. As can be seen, the entropy per unit area decreases as the alkyl chain length increases, reflecting an increased ordering of the surface monolayers for long chain alkyl molecules. Moreover, in Figure 3b, we represent the surface enthalpies for the studied ILs, and there it is apparent that this magnitude depends on temperature in an approximately linear fashion, and that it is smaller as the alkyl chain length increases as expected in less hydrogen-bonded liquids. Furthermore, it is well-known[3] that both ions of the ILs are present at the surface, so both cation and anion exert some influence on the surface tension. According to a previously reported model,[12] the charged groups point toward the bulk of the PIL and the hydrocarbon chains of the cations are exposed to air. Thus, an increase in the alkyl chain length is expected to decrease the surface tension, as observed in our results and in previously reported measurements for imidazolium-based ILs.[13] Finally, we calculated the surface thermal coefficient, $b_{T,P}$, of the studied PILs in order to analyze the effect of the degree of hydrogen bonding on the reversible extension of the surface. Prigogine and Defay[14] introduced this parameter in order to represent the heat of reversible extension of the surface at constant T and P

$$\delta Q_{rev} = C_P dT + h dP + b_{T,P} dA \quad (8)$$

where C_P and h are thermal coefficients. This parameter can be easily shown to be obtained as[15,16]

$$-b_{T,P} = \left(\frac{\partial \gamma}{\partial \ln T}\right)_{P,A} \quad (9)$$

In our case, the calculated values were 23, 16, and 10 mJ m^{-2} for EAN, PAN, and BAN, respectively, indicating also a remarkably linear dependence of the surface tension on the alkyl chain length of the cation. This behavior indicates that, as their cationic alkyl chain length increases, the ILs exert progressively lower resistance to reversible modifications of the surface area at constant T and P (a mechanical variation that involves the degree of bonding of the molecules), as expected, given the decreasing hydrogen-bonding degree for longer alkyl chains.

One of the few theoretical frameworks designed for a rational understanding of the dependence of surface tension on temperature is the phenomenological one due to Eötvös,[17] which states that $\gamma_m^{2/3} = k(T_c - T)$, where T_c is a critical temperature, V_m is the molar volume of the substance, and k is a constant value for almost all substances, typically equal to $k = 2.1 \times 10^{-7}$ (J K^{-1} $mol^{-2/3}$). If this theory was to apply to the studied ILs, one would expect that the magnitude $\gamma M^{2/3}/\rho^{2/3}$, with M being the molar mass, would show a slow linear decrease throughout the whole temperature range, and this is in fact what can be observed in Figure 4 for the compounds

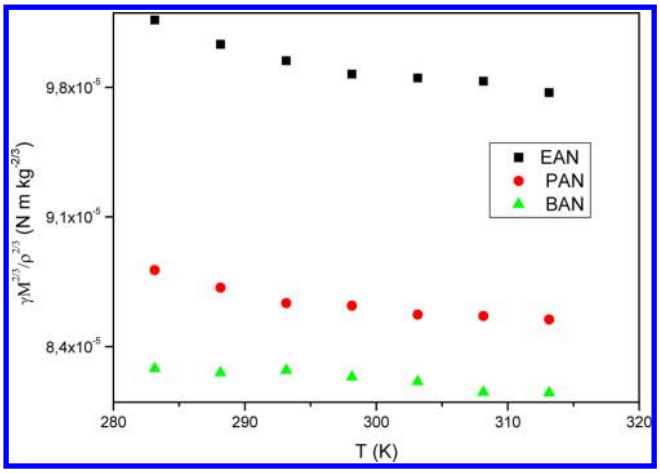

Figure 4. Temperature dependence of the Eötvös parameter for the studied PILs (see the main text).

studied here, so we could conclude that the behavior of these PILs can be approximately described by the Eötvös rule. However, a more refined result for the temperature dependence of the surface tension is due to Guggenheim[18]

$$\gamma = \gamma^0\left(1 - \frac{T}{T_c}\right)^n \quad (10)$$

where n is close to unity for metals and 11/9 for many organic liquids.[19] If one assumes, as usual, that $n \approx 1$, and that the variations of density and hence molar volume are small, then the total surface energy, E^s, will be temperature-independent, which is approximately true for liquids not too close to their critical temperatures.[20] Under these circumstances, we can write the above result as

$$\gamma = E^s\left(1 - \frac{T}{T_c}\right) \quad (11)$$

This result can be understood from a microscopic point of view in the framework of a modified harmonic oscillator model based on the one reported by Bohdansky for liquid metals, that can explain the behavior of real liquids in the region of linear thermal expansions.[20] In this formalism, which we sum up here for the interest of the reader, the pseudoreticular IL near the surface is divided into two types of cells, the ones in the surface, in which ions experience an average potential different from that in inner cells. The work for transferring an ion from the bulk to the surface is

$$W = \varepsilon_s - k_B T a \quad (12)$$

where ε_s is the external energy needed to bring an ion to the surface at $T = 0$ K, $k_B T$ is the thermal energy, and a is defined by the change in free energy per ion transition between a three-dimensional oscillator for ions in bulk cells to the corresponding harmonic potential well resembling a cell at the surface as

dx.doi.org/10.1021/jp3066822 | J. Phys. Chem. B 2012, 116, 11302−11312

$$\Delta f = k_B T a = k_B T \ln\left(\frac{\omega_b^1 \omega_b^2 \omega_b^3}{\omega_s^1 \omega_s^2 \omega_s^3}\right) \quad (13)$$

where ω_i^ξ (i = b, s; ξ =1, 2, 3) are the characteristic frequencies in bulk (b) and surface (s) cells in the three spatial directions. Thus, taking into account anharmonic effects associated with ion interactions that give rise to thermal expansions, the total surface energy is given by

$$\gamma = N(T)(\varepsilon_s - k_B T a) = N_0(1 - 2\alpha T)(\varepsilon_s - k_B T a) \quad (14)$$

This result can be rewritten in terms of the temperature of vanishing surface tension, $T^* = (\varepsilon_s/k_B a)$, usually within 10% of the real critical temperature for liquid metals, as[20]

$$\gamma = N_0 \varepsilon_s \left(1 - \frac{T}{T^*}\right)\left(1 - 2\alpha T^* \frac{T}{T^*}\right) \quad (15)$$

which, for $T \ll T^*$, can be approximated as

$$\gamma \cong N_0 \varepsilon_s \left(1 - \frac{T}{T^*}\right) \quad (16)$$

recovering Guggenheim's eq 11. Table 2 shows the values of $E^s \equiv N_0\varepsilon_s$, T^*, and $2\alpha T^*$ calculated by fitting the experimental surface tension of EAN, PAN, and BAN to the above equation. As can be seen, both the total surface energies and T^*'s monotonically increase with the alkyl chain length of the cation, as one would expect for liquids with progressively lower hydrogen bonding degrees. Moreover, the product $2\alpha T^*$ is also shown in Table 2, and must be compared to typical values in liquid alkali and alkaline earth metals ranging from 0.26 for Ba to 0.6 for Mg (see ref 20 for details).

Table 2. Surface Energies, E^s, and Temperature of Vanishing Surface Tension, T^*, for EAN, PAN, and BAN as Calculated by Fitting the Experimental Results to eq 19[a]

	E^s (mJ m^{-2})	T^* (K)	$2\alpha T^*$
EAN	74.1	926.3	1.07
PAN	55.6	1111.4	1.18
BAN	42.6	1419.3	1.47

[a]The product $2\alpha T^*$ is also shown for comparison (see the main text).

Figure 5 shows the measured values of the refractive index for the sodium yellow line (n_D) of the ILs in the studied temperature range. In addition, in Table 3, we list n_D, the Abbe numbers, ν_D, and the thermo-optic coefficient, dn_D/dt, for the three studied PILs together with the corresponding values for fused silica with a view to their possible usage as photonic materials. With regard to the Abbe number, it is well-known that refractive indices are frequency-dependent, an effect that is known as optical dispersion. Optical materials can be classified attending to this property as a function of the Abbe number, defined as

$$\nu_i = \frac{1 - n_i}{n_F - n_C}, \quad i = \text{d, D} \quad (17)$$

where n_F and n_C are the refractive indices of the materials for λ_F = 486.1 nm and λ_C = 656.2 nm, respectively. The difference between these refractive indexes, $n_F - n_C$, is known as mean dispersion, and it has been measured by means of the Abbe refractometer following the conventional procedure described elsewhere.[21] $(1 - n_i)$ is called the refractivity of the material, and subscript i usually refers to the yellow Fraunhoffer line (λ_d = 587.6 nm) or the yellow sodium line (λ_D = 589.3 nm). The more dispersive a material is, the lower values the Abbe number (ν_i) takes. Optical glasses can be classified in Crown (if $n_d > 1.6$, $\nu_d > 50$ or $n_d < 1.6$, $\nu_d > 55$) or Flint (if $n_d > 1.6$, $\nu_d < 50$ or $n_d < 1.6$, $\nu_d < 55$).[22] The proximity between the yellow Fraunhoffer line and the yellow sodium line allows us to maintain these criteria in terms of n_D and ν_D. The Abbe number was determined for the three ILs at room temperature, roughly 298 K. The calculated values are also included in Table 3, and their relative dispersions are less than 6%. For the ILs with an odd number of carbons in the alkyl chain, the Abbe number increases slowly as the carbon number does and so the material tends to be less dispersive, but data for longer alkyl chains are needed to clarify this tendency. PAN, which incorporates an odd number of alkyl groups in the cation alkyl chain, presents a lower Abbe number, and thus higher dispersive power than those of EAN and PAN. This behavior is expected, since high refractive index materials are usually more dispersive. Moreover, one can also observe in Table 3 that the studied PILs are more dispersive than silica, given the values of their refractive indexes and Abbe numbers. Finally, it must be noted that this number varies inversely with temperature. Fröba et al.[21] measured the mean dispersion from 283.15 to 313.15 K in other ILs such as [EMIM][EtSO4] (ν_D = 50.31 at 283.15 K), [EMIM][NTf$_2$] (ν_D = 43.59 at 283.15 K), and [OMA][NTf$_2$] (ν_D = 66.86 at 283.15 K), and they report variations of −2.6, −2, and −10%, respectively, in this range of temperature, as expected for the PILs observed in this paper.

On the other hand, the variation of the refractive index with temperature at constant pressure P is known as the thermo-optic coefficient:[23]

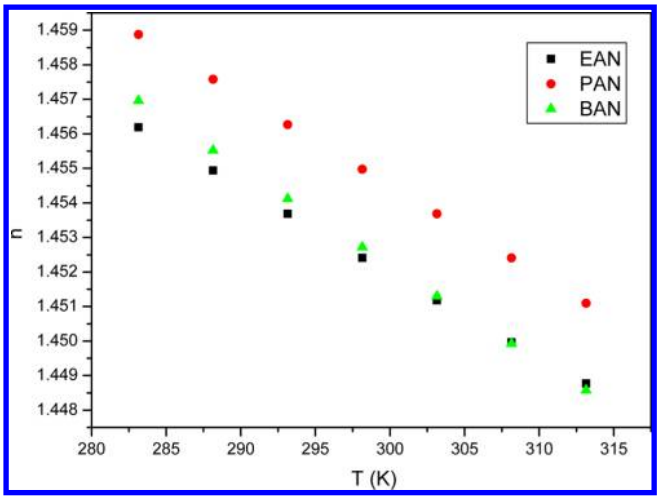

Figure 5. Temperature dependence of the refractive index of the PILs studied in this work.

Table 3. Refractive Index, n_D, Abbe Number at Room Temperature, ν_D, and Thermo-Optic Coefficient for the Yellow Line of Sodium of EAN, PAN, and BAN[a]

LI	n_D	ν_D	dn_D/dT (K^{-1})
EAN	1.4524 ± 5 × 10^{-4}	51.86	−2.41 × 10^{-4}
PAN	1.4549 ± 5 × 10^{-4}	42.8	−2.51 × 10^{-4}
BAN	1.4527 ± 5 × 10^{-4}	54.98	−2.71 × 10^{-4}
fused silica	1.4583	67.82	∼10^{-6}

[a]Data related to fused silica are inserted in order to compare the properties of these ILs with a common optical material.

dx.doi.org/10.1021/jp3066822 | J. Phys. Chem. B 2012, 116, 11302−11312

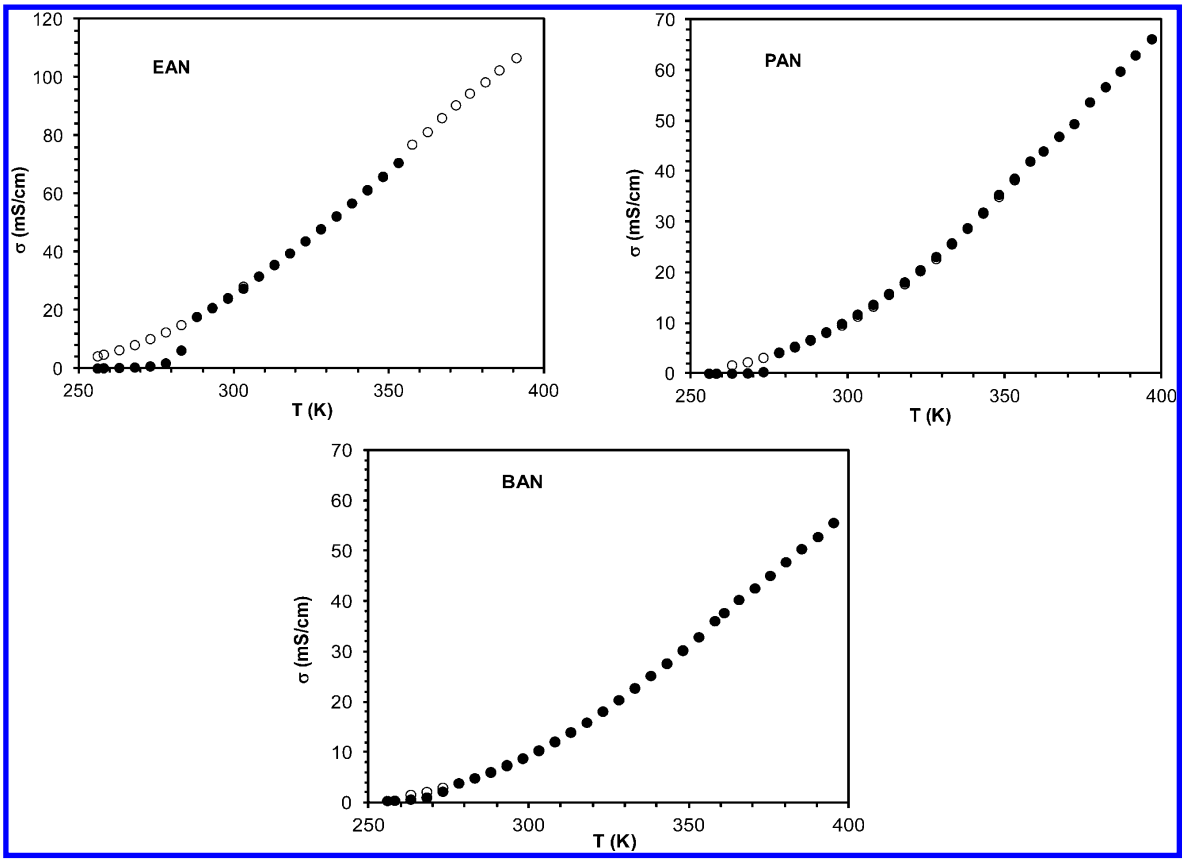

Figure 6. Behavior of the electric conductivity during the cooling−melting cycles for the PILs studied in this work. The open dots correspond to cooling, while solid dots correspond to melting.

$$\frac{dn_D(T,\rho)}{dT} = \left(\frac{\partial n_D}{\partial \rho}\right)_T \left(\frac{\partial \rho}{\partial T}\right)_P + \left(\frac{\partial n_D}{\partial T}\right)_P$$
$$= -\alpha\rho\left(\frac{\partial n_D}{\partial \rho}\right)_T + \left(\frac{\partial n_D}{\partial T}\right)_P \quad (18)$$

and in transparent materials it usually takes values between 10^{-3} and 10^{-6} K^{-1}, and it slightly depends on the wavelength of the incident light. This magnitude is the result of a delicate interplay between the thermal expansion or electrostriction (1st term on the right-hand side (rhs) of the above equation), and the thermal dependence of the electronic polarizability in conjunction with other temperature-dependent changes in the refractive index (second term on the rhs) that are less important in liquids. Positive thermal expansion coefficients induce a decrease of the slope of the refractive index vs T curve, whereas a positive change in polarizability with temperature increases it. Therefore, high thermal expansion materials usually exhibit negative thermo-optic coefficients, contrary to what could be expected for low thermal expansion materials. In ionic materials, the electrostriction term dominates over the other, and in consequence, the thermo-optic coefficients are negative.[24,25] In fact, in our case, the plots in Figure 5 exhibit a quasi-linear relation between the refractive index and temperature with a negative slope. A linear fit (r^2 = 0.9998) returns the thermo-optic coefficients for each IL, which are shown in Table 3. The radii of the confidence intervals for the coefficients at a confidence level of 95% were $\pm 2.5 \times 10^{-6}$, $\pm 3.1 \times 10^{-6}$, and $\pm 3.1 \times 10^{-6}$ for EAN, PAN, and BAN, respectively. The calculated slopes become more negative as the cationic alkyl chain length increases, so we conclude that the higher dilatation coefficients associated with lower degrees of hydrogen bonding are responsible for the dominant contribution to the thermo-optic coefficient of these PILs. This conclusion is reinforced if one takes into account that for alkanes dn/dT slowly increases with the chain length.[26]

With respect to transport variables, Figure 6 represents the electric conductivity measurements for the three PILs analyzed in this paper down to temperatures for which the electric conductivity is essentially negligible within the experimental uncertainty. As can be seen in this figure, the three studied liquids show freezing−melting hysteresis loops at the liquid−solid phase transition, in the same fashion that has been recently shown by some of the authors for ILs of the imidazolium family.[27] These hysteresis cycles are a result of the energy barriers associated with the formation of the critical nuclei necessary for both melting and solidification to take place. However, contrary to what is observed in other nonprotic imidazolium-based ILs,[27] the supercooled regions observed for C*n*AN do not end in abrupt falls of the electric conductivity, and the homogeneous nucleation temperatures (by definition, the limit of stability of the supercooled liquid) are essentially identical to those where the electric conductivity becomes that of the solid phase. This is particularly visible in the case of EAN, and it suggests that the formation of the critical nuclei could possibly be frustrated by the extensive hydrogen bonding network $^{+}NH\cdots O^{-}$ in this PIL, which is known to exert a significant influence on the supercooled dynamics of liquids by inducing high-energy barriers for nucleation.[28] Moreover, the shape of the freezing−melting hysteresis loop is seen to depend

dx.doi.org/10.1021/jp3066822 | J. Phys. Chem. B 2012, 116, 11302−11312

markedly on the length of the alkyl chain of the cation, since (i) the difference in conductivity between the supercooled liquid and the solid phase is larger for shorter chains and (ii) the width of the supercooled region (calculated as the difference between the solidification and melting temperatures) is smaller for ILs with longer cationic alkyl chains. Therefore, we conclude that the longer the cation alkyl chain, the weaker the stability of the supercooled liquid. This is once more related to the fact that the energy barriers for homogeneous nucleation are expected to increase with the amount of hydrogen bonds in the liquid.

On the other hand, Figure 7 shows the conductivity near ambient temperature together with the Arrhenius plot for the

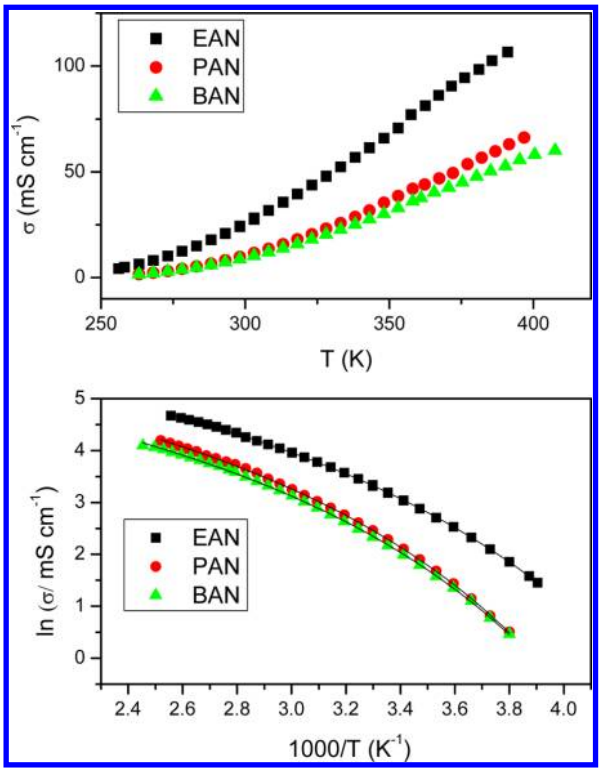

Figure 7. Temperature dependence of the conductivity (above) and Arrhenius plot (below) for the PILs analyzed in this paper. The lines shown in the lower plot correspond to the fittings to the VFT (eq 19) (parameters shown in Table 4).

conductivities of the analyzed PILs in this region, and Figure 8 presents the same plots for the viscosity. The viscosity of ILs has been reported to increase with increasing alkyl chain length, an effect normally associated with enhanced van der Waals forces.[3] Surprisingly enough, the viscosity of PAN is larger than that of BAN, while its conductivity is also larger than that of its longer chain homologue, reflecting the different mechanisms involved in mass and charge transport. Moreover, as one can see, the conductivity of these compounds increases with temperature (as expected) in a nonlinear way, giving rise to a non-Arrhenius glassy dynamics. This glass transition in the low temperature region is known to be associated with an extraordinary slowdown of the relaxation and transport mechanism,[29,30] due to the "dearth of configurations", an enormous reduction of the number of accessible microstates (configurational entropy) that takes place as the temperature falls. As a consequence, the relaxation and transport processes

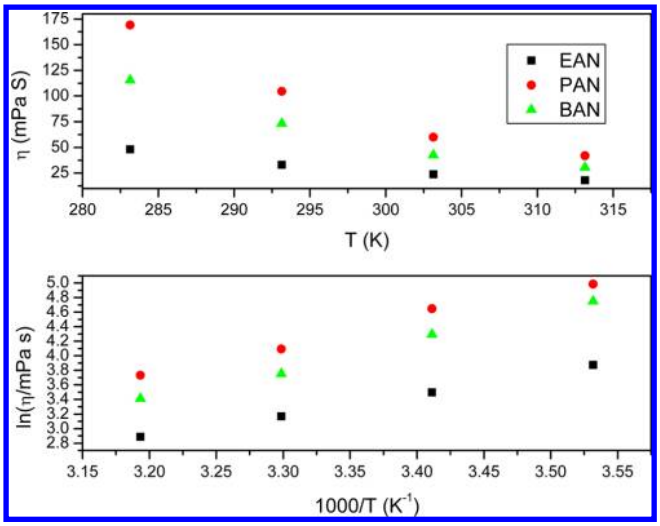

Figure 8. Temperature dependence of the viscosity (above) and Arrhenius plot (below) of the studied PILs.

suffer considerable restrictions that are universally governed by the Vogel–Fulcher–Tamman (VFT) relation:[31,32]

$$\ln \sigma = \ln \sigma_\infty - \frac{DT_0}{T - T_0} \tag{19}$$

D is called the fragility index or strength index, and it is inversely proportional to the fragility of the liquid,[33] and T_0 is the vanishing mobility temperature or Vogel temperature. As for ILs, it is now a well-known fact that transport processes in ILs usually exhibit a thermal activation of the VFT type.[34] This form of the thermal activation equation is associated with the complex underlying relaxation dynamics with several relaxation times characteristic of disordered systems, and the corresponding correlation functions are usually described by means of a stretched exponential or Kohlrausch–Williams–Watts relaxation function, $\exp[-(t/\tau)^\beta]$.[35] This is explained in the framework of Adam–Gibbs (AG) theory,[36,37] where the reduction of the available number of configurations upon cooling is associated with an increase in the size of cooperatively rearranging regions (CRR) in the liquid. According to the AG model, the Vogel temperature can be equated to the glass transition temperature for infinitely slow processes, where the glass transition becomes a true second-order phase transition.[38] This was approximately the case in this paper, since low cooling rates were used in the experiments. For $T \gg T_0$, this equation recovers the conventional Arrhenius expression, $\ln \sigma = \ln \sigma_\infty - E_A^\Lambda/k_B T$, when the activation energy of the conductivity, E_A^Λ, is the same for all the ionic hopping motions between holes. The measured data were fitted to the VFT expression, and the fitting coefficients obtained are shown in Table 3, including the effective activation energy. As it is well-known, the effective activation energy is related to the Vogel temperature and the fragility index by $B = Dk_B T_0$.[39] As can be seen, the conductivity at infinite temperature becomes lower as the alkyl chain length of the cation increases. The same trend is observed for the fragility index as the number of carbon atoms in the alkyl chain of the cation increases, but the Vogel temperature shows a maximum for PAN. Moreover, as one can see in Table 3, the fragility index and effective activation energy of PAN are slightly higher than those of BAN (although practically equal given the experimental uncertainties), reflecting a somehow

dx.doi.org/10.1021/jp3066822 | J. Phys. Chem. B 2012, 116, 11302–11312

lower fragility of PAN. This implies that PAN is a stronger liquid than BAN and, therefore, that it has an energy landscape with less potential energy minima, occupying a lower position in the hierarchy of configurational excitability. This is somehow surprising, since, as we mentioned previously, Hirao et al.[7] reported that a decrease in the cation size lowers the glass transition temperature (T_g) by decreasing the packing and cohesive energy of the salts. More specifically, for primary alkylammonium-based PILs, the glass transition temperature has been reported to increase slowly with increasing alkyl chain lengths for anion or cation. Similar nonmonotonic trends were previously reported for a closely related series like that of ethyl-, propyl-, butyl-, and pentylammonium formate,[12] in which the melting temperatures of ethyl- and butylammonium formates are lower than those of the other members of the series. If this trend is associated with the existence of an odd number of carbon atoms in the cationic alkyl chains has to be proved analyzing the next member of the alkylammonium nitrate family, and reducing the experimental and computational uncertainties.

As shown in the fragility plot in Figure 9, the same conclusion can be reached from the analysis of the viscosity

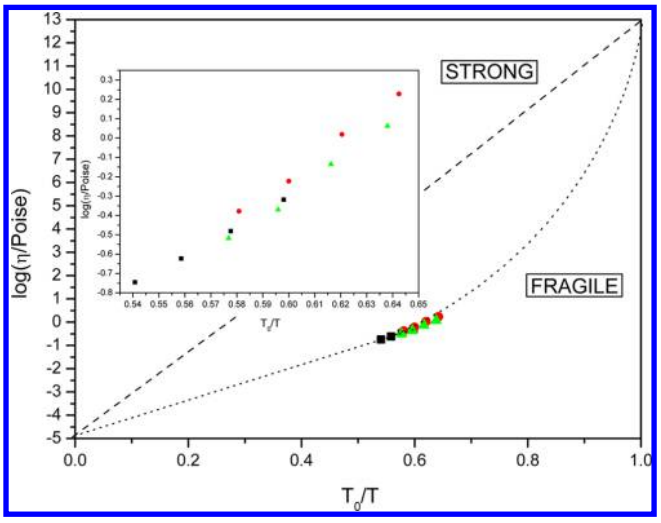

Figure 9. Fragility plot for the studied PILs. The inset shows the experimental data in the studied temperature range.

data, where we can see that PAN is slightly stronger than BAN, which is in turn a little more fragile than EAN, reflecting the lower hydrogen bonding degree of BAN.[39] Once more, one must recall that chains with an odd number of carbon atoms pack worse than their even-numbered counterparts, so they are expected to give rise to less structured environments in the bulk IL, and that could possibly be the reason behind the somehow anomalous behavior of PAN. Moreover, all the hereby studied PILs belong to the intermediate region of the fragility scale, as PILs are known to.[40] As it is well-known, fragility is a measure of the thermal sensitivity of the liquid structure. The glassy structures of "fragile" liquids collapse under subtle variations of the temperature, changing to states of considerable fluctuation of the structural arrangement and coordination states.[40] These liquids are in contrast with the so-called "strong" liquids, which show greater resistance to structural rearrangements even under wide variations of temperature.

Moreover, we have specifically analyzed the high temperature data of both conductivity and viscosity, where approximately Arrhenius behavior is expected, and the parameters are shown in Table 5. As can be seen in this table, the limiting conductivities follow the same trend as that detected in the complete VFT fits, and the activation energies exhibit the same inversion for PAN, since for this compound the activation energy is greater than that for BAN. Moreover, Table 5 compares the activation energies obtained from the fits to Arrhenius-like equations of both the conductivity and viscosity experimental measurements. As both activation energies are not equal, the Walden equation $\Lambda\eta = cte$ is not followed, and thus, the mechanism of electric conduction by these liquids cannot be considered completely ionic or electrophoretic. The Walden rule is often obeyed by ionic solutions of large and weakly coordinating ions in solvents with nonspecific ion−solvent interactions, where ion migration is the only mechanism behind ion mobility and electric conductivity. However, in dense ionic systems, deviations from the conventional Walden rule are registered, due to ionic association and other correlations that influence conductivity. Particularly, ILs are normally well under the ideal line typical of highly diluted, totally dissociated, strong electrolyte solutions, as can be seen in Figure 10 for the

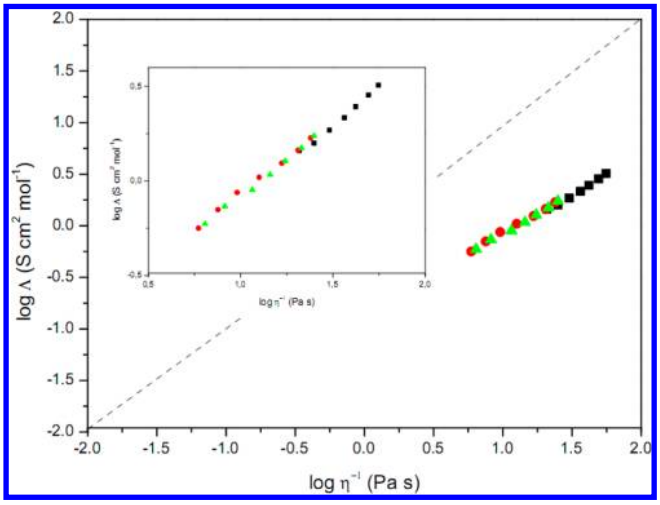

Figure 10. Walden plot of the studied PILs. The inset shows the experimental data in the studied temperature range.

Table 5. Fitting Parameters of Experimental Conductivity and Viscosity of the Studied PILs to Arrhenius Equations

	conductivity		viscosity			
	$\ln \sigma_\infty$ (mS cm^{-1})	E_A^Λ (kJ mol^{-1})	$\ln \eta_\infty$ (mPa s)	E_A^η (kJ mol^{-1})	$\varsigma^{\text{Walden}}$	$\varsigma = \frac{E_A^\Lambda}{E_A^\eta}$
EAN	11.21 ± 0.16	19.87 ± 0.54	−6.46 ± 0.22	24.26 ± 1.91	0.83 ± 0.03	0.83 ± 0.07
PAN	12.97 ± 0.23	26.50 ± 0.54	−8.45 ± 0.97	31.66 ± 2.40	0.75 ± 0.02	0.84 ± 0.06
BAN	12.59 ± 0.18	25.89 ± 0.42	−9.5 ± 0.66	33.49 ± 1.66	0.77 ± 0.02	0.77 ± 0.04

dx.doi.org/10.1021/jp3066822 | J. Phys. Chem. B 2012, 116, 11302−11312

presently reported PILs. Specifically, this subionic behavior—associated with small populations of ions or low degrees of ionicity[39]—has been abundantly reported in the literature for PILs (see, e.g., Belieres and Angell,[39] MacFarlane et al.,[40] or Yoshizawa et al.[41]). Moreover, recently the Walden plot has been generalized for ILs to the so-called fractional Walden rule, $\Lambda\eta^{\zeta} = C$, where C is a temperature-dependent constant known as the Walden product. The slope of the fractional Walden plot, ζ, is related to the degree of association of the ions, and must be approximately equal to the ratio of the activation energies of conductivity and viscosity. This is seen to be the case for the studied PILs, since ζ values calculated from the Walden plot are in good agreement with those obtained from the conductivity and viscosity Arrhenius analysis (see Table 5). Once again, in order to rationalize the observed behavior of the ionicity, one must recall that these systems are highly nanostructured materials. Nanoscale heterogeneities are mainly due to solvophobic interactions between alkyl groups, so they are enhanced as the number of carbon atoms in the molecular architecture of the ions is increased, but electrostatic and hydrogen bonding also play important roles in the nanostucturing of the bulk mixture.[42] The existence of persistent nanostructure is known to provoke a decrease of the mobility of the ions in the bulk IL.[43] This is compatible with our observation that BAN has the lowest conductivities of the studied series. However, the slightly higher viscosity of PAN induces a somewhat larger ionicity of this compound, although the differences are very small in this case. This is probably associated with the fact that alkane chains with an odd number of carbon atoms are known to pack worse than their even-number counterparts.

Table 4. Fitting Parameters of the Experimental Conductivity of the Studied PILs to the VFT Equation (eq 19)

LI	A (S cm^{-1})	D	T_0 (K)	B (kJ mol^{-1})
EAN	87.99 ± 1.95	2.73 ± 0.05	169.34 ± 0.83	3.84
PAN	64.17 ± 1.91	2.67 ± 0.06	181.90 ± 0.98	4.04
BAN	52.38 ± 2.08	2.65 ± 0.08	180.65 ± 1.41	3.98

CONCLUSIONS

In the present paper, we report a systematic study of the effect of the cationic chain length on several equilibrium and transport properties of the first members of the alkylammonium nitrate PIL family (ethylammonium, propylammonium, and the newly synthesized butylammonium nitrate) in the temperature range between 10 and 40 °C. We measured densities and sound velocities, calculating the dilatation coefficients and compressibilities. Rao's coefficients have also been a matter of study, and they were seen to increase with the alkyl chain length, and also slightly with temperature for each compound. Surface tension was analyzed, and we calculated the surface entropies and enthalpies proving that the temperature dependence of the surface tension can be adequately understood using the Guggenheim equation, which can be deduced from a modified harmonic oscillator model for pseudolattice ILs. The surface energies and temperatures of vanishing surface tension increase as the alkyl chain length increases, reducing the degrees of hydrogen bonding, and the behavior of the surface thermal coefficients is also adequately explained with this reduction. Besides, refractometry measurements proved that the refractive index of PAN is higher than those of the other two studied PILs, and that of BAN is even lower than the one corresponding to EAN at high temperatures. Moreover, the Abbe number at room temperature exhibits a minimum for PAN in the studied series. Notwithstanding these seemingly anomalous behaviors, the thermo-optic coefficient displays a monotonic decrease with the alkyl chain length in marked contrast to what happens in alkanes, reflecting that in these cases the influence of the electrostrictive contribution dominates over the thermal dependence of the polarizability. Likewise, transport properties such as conductivity and viscosity were measured and the influence of the cationic chain length in the supercooled liquid region analyzed. Hysteresis loops were seen to exist for solidification−melting cycles of these PILs, and the effect of the length of the alkyl chain length of the cation on the size of the loop analyzed, showing that longer chains lead to a narrowing of the supercooled region. Moreover, the temperature dependence of the conductivity was studied in the Vogel−Fulcher−Tamman (VFT) framework, obtaining fragility indexes, effective activation energies, and Vogel temperatures. Once again, PAN was seen to have a somewhat different behavior, proving to be the strongest of the three studied PILs. All the studied systems were found to be subionic and fragile liquids by means of the fragility and Walden plots, respectively, with PAN exhibiting the lowest fragility and the highest ionicity of all the studied compounds. All the reported observations are compatible with a decrease of the degree of hydrogen bonding and a more persistent nanostructure in the bulk mixtures due to enhanced hydrophobic interactions with the cationic chain length of the PILs. The analysis of the solvation mechanisms of dissolved inorganic salts and their influence on the physical properties of these ILs is currently in progress.

AUTHOR INFORMATION

Corresponding Author

*E-mail: luismiguel.varela@usc.es.

Notes

The authors declare no competing financial interest.

ACKNOWLEDGMENTS

The authors wish to thank the financial support of Xunta de Galicia through the research projects of references 10-PXI-103-294 PR and 10-PXIB-206-294 PR. All of these research projects are partially supported by FEDER funds. J.C. and T.M.-M. thank the Spanish ministry of Education for their FPU grants.

REFERENCES

(1) Wilkes, J. S.; Zaworotko, J. *J. Chem. Soc., Chem. Commun.* **1992**, 965−967.
(2) Patrascu, C.; Gauffre, F.; Nallet, F.; Bordes, R.; Oberdisse, J.; de Lauth Viguerie, N.; Mingotaud, C. *ChemPhysChem* **2006**, *7*, 99−101.
(3) Greaves, T. L.; Drummond, C. J. *Chem. Rev.* **2008**, *108*, 206−237.
(4) Bordel Velasco, S.; Turmine, M.; Di Caprio, D.; Letellier, P. *Colloids Surf., A* **2006**, *275*, 50−54.
(5) Fernández-Castro, B.; Méndez-Morales, T.; Carrete, J.; Fazer, E.; Cabeza, O.; Rodríguez, J. R.; Turmine, M.; Varela, L. M. *J. Phys. Chem. B* **2011**, *115*, 8145−8154.
(6) Greaves, T. L.; Kennedy, D. F.; Mudie, S. T.; Drummond, C. J. *J. Phys. Chem. B* **2010**, *114*, 10022−10031.
(7) Hirao, M.; Sugimoto, H.; Ohno, H. *J. Electrochem. Soc.* **2000**, *147*, 4168−4172.
(8) Rao, R. *Indian J. Phys.* **1940**, *14*, 109−116.

(9) Nozdrev, V. Z. *The Use of Ultrasonics in Molecular Physics*; McMillan: New York, 1965.
(10) Hartmann, B. *J. Acoust. Soc. Am.* **1979**, *65*, 1392−1396.
(11) Madigosky, W. M.; Rosenbaum, I.; Lucas, R. *J. Acoust. Soc. Am.* **1981**, *69*, 1639−1643.
(12) Greaves, T. L.; Weerawardena, A.; Fong, C.; Krodkiewska, I.; Drummond, C. J. *J. Phys. Chem. B* **2006**, *110*, 22479−22487.
(13) Rilo, E.; Domínguez-Pérez, M.; Vila, J.; Varela, L. M.; Cabeza, O. *J. Chem. Thermodyn.* **2012**, *49*, 165−171.
(14) Defay, R.; Prigogine, I. In *Surface tension and adsorption*; Longmans, Green & Co. Ltd.: London, 1966; pp 36−38.
(15) Turmine, M.; Duvivier, S.; Mayaffre, A.; Letellier, P. *J. Phys. Chem. B* **2003**, *107*, 125−129.
(16) Malham, I. B.; Letellier, P.; Turmine, M *J. Phys. Chem. B* **2006**, *110*, 14212−14214.
(17) Eötvös, L. *Ann. Phys.* **1886**, *27*, 448−459.
(18) Guggenheim, E. A. *J. Chem. Phys.* **1945**, *13*, 253−261.
(19) Adamson, A. W.; Gast, A. P. *Physical Chemistry of Surfaces*, 6th ed.; Wiley: New York, 1997; p 50.
(20) Bohdansky, J. *J. Chem. Phys.* **1968**, *49*, 2982−2986.
(21) Fröba, A. P.; Kremer, H.; Leipertz, A. *J. Phys. Chem. B* **2008**, *112*, 12420−12430.
(22) Smith, W. *Modern Optical Engineering*; McGraw-Hill: New York, 1966.
(23) Prod'homme, L. *Phys. Chem. Glasses* **1960**, *1*, 119−122.
(24) Ghosh, G. *Handbook of Thermo-Optic Coefficients of Optical Materials with Applications*; Academic Press: New York, 1998; p 199.
(25) Palik, E. D. Thermooptic coefficients. *Handbook of optical contants of solids*; Academic Press: San Diego, CA, 1991.
(26) Kaplan, S. G.; Burnett, J. H. *Appl. Opt.* **2006**, *45*, 1721−1724.
(27) Vila, J.; Fernández-Castro, B.; Rilo, E.; Carrete, J.; Domínguez-Pérez, M.; Rodríguez, J. R.; García, M.; Varela, L. M.; Cabeza, O. *Fluid Phase Equilib.* **2012**, *320*, 1−10.
(28) Roland, C. M.; Casalini, R.; Bergman, R.; Mattsson, J. *Phys. Rev. B* **2008**, *77*, 012201(1)−012201(4).
(29) Angell, C. A. In *Complex Behaviour of Glassy Systems*; Rubí, M., Pérez-Vicente, C., Eds.; Springer: Berlin, 1997.
(30) Kitamura, T. *Phys. Rep.* **2003**, *383*, 1−94.
(31) Vogel, H. *Phys. Z.* **1921**, *22*, 645−646.
(32) Tamman, G.; Hesse, W. *Z. Anorg. Allg. Chem.* **1926**, *156*, 245−257.
(33) Böhmer, R.; Ngai, K. L.; Angell, C. A.; Plazek, D. J. *J. Chem. Phys.* **1993**, *99*, 4201−4209.
(34) Vila, J.; Gines, P.; Pico, J. M.; Franjo, C.; Jimenez, E.; Varela, L. M.; Cabeza, O. *Fluid Phase Equilib.* **2006**, *242*, 141−146.
(35) Metatla, N.; Soldera, A. *Macromolecules* **2007**, *40*, 9680−9685.
(36) Adam, G.; Gibbs, J. H. *J. Chem. Phys.* **1965**, *43*, 139−146.
(37) Gibbs, J. H.; DiMarzio, E. A. *J. Chem. Phys.* **1958**, *28*, 373−383.
(38) Martinez, L. M.; Angell, C. A. *Nature (London)* **2001**, *410*, 663−667.
(39) Belieres, J.-P.; Angell, C. A. *J. Phys. Chem. B* **2007**, *111*, 4926−4937.
(40) MacFarlane, D. R.; Forsyth, M; Izgorodina, E. I.; Abbott, A. P.; Annat, G.; Fraser, K. *Phys. Chem. Chem. Phys.* **2009**, *11*, 4962−4967.
(41) Yoshizawa, M.; Xu, W.; Angell, C. A. *J. Am. Chem. Soc.* **2003**, *125*, 15411−15419.
(42) Atkin, R.; Warr, G. G. *J. Phys. Chem. B* **2008**, *112*, 4164−4166.
(43) Yan Shen; Kennedy, D. F.; Greaves, T. L.; Weerawardena, A.; Mulder, R. J.; Nigel Kirby, N.; Song, G.; Drummond, C. J. *Phys. Chem. Chem. Phys.* **2012**, *14*, 7981−7992.